SIAM J. APPL. MATH.
Vol. 66, No. 5, pp. 1610–1631

INTERACTION OF ADVANCING FRONTS AND MENISCUS PROFILES FORMED BY SURFACE-TENSION-GRADIENT-DRIVEN LIQUID FILMS*

P. L. EVANS† AND ANDREAS MÜNCH‡

Abstract. On a tilted heated substrate, surface tension gradients can draw liquid up out of a reservoir. The resulting film thickness profile is controlled by two parameters, which depend on the tilt of the substrate, the imposed temperature gradient, and the thickness of a postulated thin precursor layer. The evolution of this film in time is studied using a lubrication model. A number of distinct behaviors are possible as the substrate tilt angle and other parameters are varied. Recent results for the multiple stationary profiles possible near the meniscus are used, and the interaction of these profiles with the advancing front is examined. We demonstrate how to systematically determine the evolution of the entire film profile from the meniscus to the apparent contact line. This allows a categorization of the range of behaviors for a transversely uniform profile in a two-dimensional parameter space. In addition to capillary fronts and double shock structures, new combinations that arise for certain ranges of large substrate tilt and precursor thickness are described. These include profiles involving rarefaction fans, connecting to either an undercompressive or a classical wave at the advancing front.

Key words. lubrication theory, Marangoni shear stress, capillarity, traveling waves

AMS subject classifications. 76D08, 35Q35, 76A20, 76D45, 35G25, 34E05

DOI. 10.1137/050625242

1. Introduction.

In this paper we consider the time-dependent behavior of a thin liquid film on a tilted heated substrate. Such a film is produced when a temperature difference is imposed along a substrate with one end immersed into a reservoir containing a liquid such as silicone oil, giving rise to a surface tension gradient. The resulting surface shear stress drags liquid up from the reservoir, while gravitational forces act to return liquid to the reservoir. This may give rise to a film of liquid which climbs up the substrate. The evolution of the film above the reservoir has received considerable attention in recent years [11, 12, 16]. An understanding of thin-film flows driven by surface tension gradients is of importance, for instance, in "Marangoni drying" [9] and controlling flows in microfluidic applications [6].

Experiments (e.g., by Schneemilch and Cazabat [14, 15]) reveal that the film tends to advance with a steep front at a contact line, where the liquid-air interface meets the substrate. Previous studies have considered the film behavior in the vicinity of the meniscus and at the advancing front independently of each other. The advancing front can be a simple compressive one or an undercompressive shock as part of a double wave structure [2, 11]. Furthermore, it is known that at the meniscus, multiple film profiles are possible. For a fixed combination of substrate inclination and shear stress, the meniscus can settle into either of basically two different profiles [13]. In

*Received by the editors February 24, 2005; accepted for publication (in revised form) February 23, 2006; published electronically June 9, 2006. This work was supported by the DFG Research Center MATHEON (Project C10) in Berlin.

http://www.siam.org/journals/siap/66-5/62524.html

†Humboldt University of Berlin, Institute of Mathematics, Unter den Linden 6, D-10099 Berlin, Germany (pevans@mathematik.hu-berlin.de).

‡Weierstrass Institute for Applied Analysis and Stochastics (WIAS), Mohrenstraße 39, D-10117 Berlin, Germany (muench@mathematik.hu-berlin.de). This author was supported by a Heisenberg Fellowship.

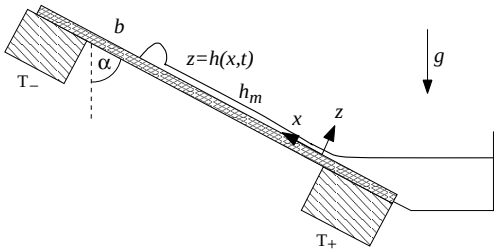

FIG. 1.1. *The thin film on a heated tilted substrate rises from a meniscus. Two heaters hold the temperature at the ends of the substrate at temperatures $T_+ > T_-$. The resulting Marangoni shear stress drives a thin liquid film of thickness $h(x,t)$ up the substrate. At the front, the film advances over a thin precursor layer of thickness b (not shown).*

this paper we determine which meniscus profiles are linked with which traveling wave profiles, and how this link occurs, i.e., which are selected. In the sense that this is a composite description, this work is in the spirit of earlier work by Hocking [7] on the connection between a moving contact line and the meniscus during withdrawal of a moving substrate, which is closely related to the present work. The picture that emerges here for the Marangoni-driven film is, however, more complicated, since we have to include the additional possibility arising from structures involving nonclassical waves in our investigation.

As in our earlier work [13], we consider the arrangement shown in Figure 1.1. The substrate is held at an angle α measured from the vertical, and it is heated so as to impose a uniform temperature gradient $(\mathrm{d}T/\mathrm{d}x) = \gamma < 0$ along the substrate. The film surface tension is σ at some reference temperature, and $\sigma_T = (\mathrm{d}\sigma/\mathrm{d}T) < 0$ is the sensitivity of the surface tension to temperature changes. The shear stress is then $\tau = \gamma\sigma_T$. The film density is ρ, and g is the acceleration due to gravity. We begin section 2 with a statement of the equations governing the film evolution. We then review the evolution of the film at the meniscus and advancing front, considered individually. The former area has been the subject of extensive investigations by us [11, 13] and others, and the latter by Münch, Bertozzi, and others [2, 10].

The dimensionless parameter D was introduced by Bertozzi, Münch, and Shearer [2]. It is a measure of both the substrate angle α and the strength of the surface shear stress driving the flow. Thus

$$D = \left(\frac{3\delta}{\cos^2\alpha}\right)^{2/3} \sin\alpha, \quad \text{where } \delta = \frac{\tau}{2\sqrt{\sigma\rho g}}. \tag{1.1}$$

Bertozzi, Münch, and Shearer [2] define their substrate angle as the complement of α, but their definition of D is equivalent to (1.1). For large inclinations from the vertical (and fixed shear stress) the parameter D is relatively large, and in this case the normal component of gravity is important. A distinct separation between the meniscus and a structure at the advancing front occurs in most circumstances. We build on earlier work, including our preliminary investigation [13], by systematically considering the possible interactions between these structures, and we describe what structures can arise, and the connections between them, in section 3. The combined picture we present is confirmed by dynamical simulations. We also extend previous work by considering the large D limit in section 4. In this case we find that the film can no longer be thought of as separate meniscus and front structures; instead the

film smoothly varies from one to the other without a flat region. The result of our investigations in sections 3 and 4 is a coherent picture of the film behavior as D and the thickness of a presumed precursor layer are varied, which we present in section 5. Finally section 6 summarizes our work.

2. Preliminaries.

2.1. Formulation. We denote the time-dependent film thickness profile by $h(x,t)$, where x measures distance up the substrate and t is time. Using ideas from singular perturbation theory, an evolution equation governing $h(x,t)$ may be obtained [11]. This governing equation is

$$h_t + \Omega_x (h^2)_x - (h^3)_x = -(h^3 \kappa_x)_x + D(h^3 h_x)_x, \tag{2.1}$$

where $\kappa = h_{xx}(1+\epsilon^2 h_x)^{-3/2}$ is the nonlinear expression for the curvature of the free surface. Here $\epsilon = H/L$ (where H and L are given below) is a small parameter, and so $\epsilon \ll 1$. In (2.1), Ω is a dimensionless temperature profile for which $\Omega_x = 1$ except near the heaters, where Ω becomes constant, cutting off surface tension gradients there. Equation (2.1) is obtained by scaling h, x, and t by

$$H = \frac{3\tau}{2\rho g \cos\alpha}, \quad L = \left(\frac{3\sigma\tau}{2\rho^2 g^2 \cos^2\alpha}\right)^{1/3}, \quad T_0 = 2\mu\left(\frac{4\sigma\rho g\cos\alpha}{9\tau^5}\right)^{1/3},$$

respectively. The terms in h^2 and h^3 on the left-hand side of (2.1) account for the competing effects of the imposed shear stress and drainage due to the component of gravity parallel to the substrate. The first term on the right-hand side is due to surface tension, which is supposed to not differ appreciably from its reference value, except inasmuch as it provides the driving shear stress. The second arises from the leveling effect of the component of gravity normal to the substrate. It is useful to define the flux function, $f(h) = h^2 - h^3$, which represents the flux of liquid up the substrate in the absence of the second- and fourth-order smoothing terms in (2.1).

As explained in our earlier work [13], when $\epsilon = H/L = (9\delta^2/\cos\alpha)^{1/3} \ll 1$, it is appropriate to replace κ by the approximate expression h_{xx} in the thin film region away from the reservoir. In addition, when $\epsilon \ll D$ it follows that $\epsilon|h_x| \ll 1$ in the vicinity of the reservoir, and approximating κ by h_{xx} is also appropriate there. We set $\Omega_x \equiv 1$, requiring that as α is increased the position of the heater is moved further into the reservoir, i.e., towards large negative x values. In this way a uniform temperature gradient, and hence uniform shear stress, is imposed. Equation (2.1) then reduces to

$$h_t + (h^2 - h^3)_x = -(h^3 h_{xxx})_x + D(h^3 h_x)_x. \tag{2.2}$$

An appropriate boundary condition at the meniscus is that the film profile flattens out to meet the undisturbed reservoir, so $\partial h^*/\partial x^* \sim -\cot\alpha$ in dimensional units. After rescaling, this yields

$$h \sim -x/D \qquad \text{as } x \to -\infty. \tag{2.3}$$

To avoid the singularity associated with a moving contact line, we adopt a precursor model so

$$h \to b \qquad \text{as } x \to \infty \tag{2.4}$$

and define the apparent contact line to be the point where the film thickness first becomes approximately b.

We are concerned with the behavior of solutions of (2.2) subject to (2.3) and (2.4). Solutions of (2.2)–(2.4) are potentially influenced by just two parameters, D defined by (1.1) above and the precursor layer thickness, b. A particular combination of these parameters determines the structure of the climbing film, including the meniscus. In the following sections, we enumerate and describe the possible film structures.

Solutions of (2.2) typically have two distinct parts, a meniscus and a wave structure consisting of one or two advancing waves. Near the reservoir the meniscus part settles into an equilibrium solution with thickness approaching some value h_m. Immediately behind the moving apparent contact line, where the film abruptly decreases to the precursor, is a traveling wave, which we refer to as the "advancing front." Behind it may be additional waves that, together with the advancing front, make up the moving wave structure.

A good guide to the possible behavior of the complete film comes from considering what happens in the two parts independently. In the remainder of this section, we first describe the waves near the contact line. Here the resulting wave structure is determined by a left thickness h_w, together with D and b. We then (in section 2.3) summarize what limiting meniscus thicknesses h_m are possible for a given D. We assume that the precursor thickness b is the smallest thickness scale that appears in the film profile, and so we consider only cases where $h_w > b$.

2.2. Advancing front behavior. The wave dynamics that arise at and behind the rising contact line have been investigated in detail in recent years [1, 2, 10] by considering solutions of (2.2) with initial data that connect flat left and right states where the film profile thicknesses are h_w and b, respectively. To capture the large scale structure of the emerging waves, we rescale $x = x^*/\lambda$ and $t = t^*/\lambda$ in (2.2) and let $\lambda \to 0$. We find that (2.2) is a nonlinear perturbation of the scalar conservation law (dropping the asterisks),

$$h_t + [f(h)]_x = 0, \qquad f(h) \equiv h^2 - h^3. \tag{2.5}$$

We first discuss the situation when (2.5) is considered as the limit of the problem with exclusively nonlinear second-order diffusion, i.e., of the equation

$$h_t + [f(h)]_x = (h^3 h_x)_x. \tag{2.6}$$

One quickly finds that traveling wave solutions of (2.6) with left and right far-field conditions $h_w > b$ and b, respectively, exist precisely if $h_w \le h_{\rm int} \equiv (1-b)/2$. In the limit of vanishing second-order diffusion, these traveling waves correspond to shock solutions of (2.5), i.e., jump discontinuities

$$h(x,t) = \begin{cases} h_w & \text{if } x < st, \\ b & \text{if } x > st, \end{cases} \tag{2.7}$$

that move according to the Rankine–Hugoniot condition,

$$s = s(h_w, b) = (f(h_w) - f(b))/(h_w - b). \tag{2.8}$$

If, however, $h_w > h_{\rm int}$, a double wave structure forms, which corresponds to a rarefaction-shock solution of (2.5),

$$h(x,t) = \begin{cases} h_w & \text{if } x \le f'(h_w)t, \\ f'^{-1}(x/t) & \text{if } f'(h_w)t \le x \le f'(h_{\rm int})t, \\ b & \text{if } x \ge st, \end{cases} \tag{2.9}$$

where the speed $s = s(h_{\rm int}, b)$ of the shock between the intermediate height $h_{\rm int}$ and b also satisfies $s = f'(h_{\rm int})$.

This solution structure is consistent with the classical theory of conservation laws, which admits only Lax (also called compressive) shocks in solutions of (2.5), i.e., shocks that satisfy the Lax entropy condition

$$f'(b) < s < f'(h_w), \tag{2.10}$$

which stipulates that characteristics from both states must cross the shock trajectory, or at most the limits of Lax shocks, sometimes called *generalized Lax* shocks, where one of the inequalities is replaced by an equality. The shock in (2.9) is an example of a generalized Lax shock.

Returning to the situation where (2.5) is considered to be the limit problem of (2.2), we find that new combinations of waves that include nonclassical undercompressive shocks which violate (2.10) arise for $D = 0$, i.e., pure fourth-order diffusion, and for a range of $D > 0$. These waves have been studied in detail for $D = 0$ by Bertozzi, Münch, and Shearer [2] and for general D by Münch [10]. This investigation was carried out via numerical simulations of (2.2) and by systematic determination of the traveling wave solutions $h(x,t) = h(\xi)$, $\xi = x - st$ with far-field states h_- as $\xi \to -\infty$ and b as $\xi \to \infty$. Inserting this ansatz into (2.2), we obtain, after integrating once and using the far-field condition, the third-order ODE

$$h''' = -Dh' + f(h) - f(b) - s(h - b), \qquad ' \equiv {\rm d}/{\rm d}\xi, \tag{2.11}$$

with the wave speed $s = s(h_-, b)$ given by (2.8). This ODE was systematically investigated via phase space methods [2, 3, 10]. Traveling wave profiles appear as heteroclinic connections between the equilibria of (2.11), formed by the intersections of invariant manifolds. These can be computed numerically by following individual trajectories on the manifolds, and the intersections of invariant manifolds can be tracked (as b is varied) in Poincaré sections.

We now summarize the results of these studies on the solution of (2.2) connecting h_w and b. For $D = 0$ and a fixed value for $b < 1/3$, four different situations arise as $h_w > b$ is increased. For $b < h_w < h_{ii}(b)$, with a b-dependent upper bound, a compressive wave arises. In contrast to the case of second-order diffusion, which smooths the shock to a monotonic profile, the fourth-order diffusion induces a capillary ridge (see Figure 2.1, lower left corner). Furthermore, in a thin region $h_i(b) < h_w < h_{ii}(b)$, multiple traveling wave solutions of (2.2) exist that correspond to the same compressive shock. These waves differ by the width of their capillary ridge. Furthermore, for $1 - h_{\rm uc} - b < h_w < h_{ii}(b)$, double shocks composed of a Lax and an undercompressive shock are also possible; $h_{\rm uc}$ and undercompressive shocks are explained below. However, for $h_w < h_{ii}(b)$, monotonic initial data for (2.2) typically gives rise to the compressive wave with the smallest capillary ridge. For $h_{ii}(b) < h_w < h_{\rm uc}(b)$ a double shock results,

$$h(x,t) = \begin{cases} h_w & \text{if } x \le s(h_w, h_{\rm uc})t, \\ h_{\rm uc} & \text{if } s(h_w, h_{\rm uc})t \le x \le s(h_{\rm uc}, b)t, \\ b & \text{if } x \ge s(h_{\rm uc}, b)t, \end{cases} \tag{2.12}$$

where the trailing shock that connects the states h_w and $h_{\rm uc}$ is a Lax shock, and the leading shock from $h_{\rm uc}$ to b is undercompressive; i.e., it violates the Lax entropy condition (2.10) in that characteristics only enter from the right. The undercompressive

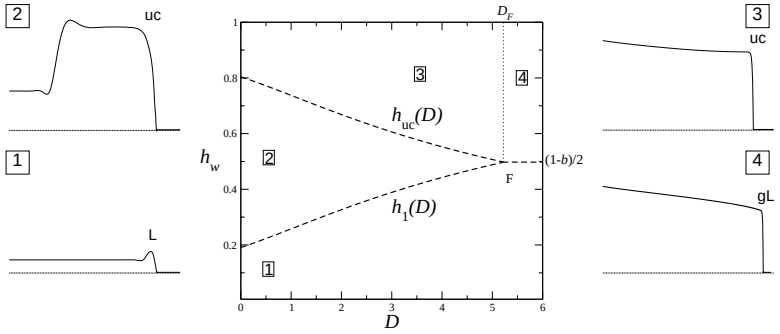

FIG. 2.1. *The front wedge diagram for $b = 0.005$ showing the four possible types of advancing front behavior, depending on D and the left state value h_w. Surrounding subfigures show qualitatively the behavior observed in each of regions 1 to 4: region 1—compressive front; 2—double shock structure (compressive and undercompressive waves); 3—rarefaction fan and undercompressive front; 4—rarefaction fan and generalized Lax shock. These regions are described further in the text. Labels indicate the type of front: L—Lax shock; uc—undercompressive shock; gL—generalized Lax shock.*

wave arises as a codimension one intersection of invariant manifolds for (2.11) and for a given b (and D) appears only for a specific value of the left state, $h_{\rm uc}$. (In contrast, compressive waves arise as codimension zero intersections.) In practice, a shooting method allows easy computation of $h_{\rm uc}(D, b)$ and hence the shape of the wedge. The trailing wave moves at a slower speed, so that the width of the plateau separating the two waves grows in time. The profile of a numerical solution of (2.2) corresponding to such a double shock is shown in the upper left corner of Figure 2.1. The emergence of nonclassical undercompressive shocks as one passes a certain threshold for h_w has been interpreted as "nucleation" [8].

For $h_w > h_{\rm uc}$, we get a rarefaction-undercompressive shock wave combination,

$$h(x,t) = \begin{cases} h_w & \text{if } x \le f'(h_w)t, \\ f'^{-1}(x/t) & \text{if } f'(h_w)t \le x \le f'(h_{\rm uc})t, \\ h_{\rm uc} & \text{if } f'(h_{\rm uc})t \le x \le s(h_{\rm uc}, b)t, \\ b & \text{if } x \ge s(h_{\rm uc}, b)t. \end{cases} \tag{2.13}$$

Note that since the shock is undercompressive, i.e., $f'(h_{\rm uc}) < s(h_{\rm uc}, b)$, it separates from the leading edge of the trailing rarefaction wave. The upper right corner of Figure 2.1 shows the corresponding solution of the full PDE (2.2).

The results for general values of D as described by Münch [10] may be summarized in a two-dimensional diagram that displays, for each D, the values of left states h_w where the different types of wave or waves connecting this state to the precursor right state b exist. In the (D, h_w) plane, the boundaries between these different ranges essentially form a wedge-like shape, shown in Figure 2.1 for the precursor thickness $b = 0.005$. This shape is defined by the graphs of $h_{\rm uc}(D, b)$ (at the upper edge) and $h_1(D, b) = 1 - h_{\rm uc} - b$ (lower edge). We refer to this shape as the "front wedge."

Because $h_{\rm uc}$ depends on b, the shape and position of the front wedge on a (D, h_w) diagram also depends on b. The apex of the wedge (shown as F in Figure 2.1) is located at $(D_F, (1-b)/2))$, where D_F is itself a monotonically decreasing function of b. The significance of this will become apparent in section 3. The two sides of the wedge, together with the extension of the wedge's apex $\{(D, h) : D > D_F,\ h = (1-b)/2\}$ and the line $\{(D, h) : D = D_F,\ h > (1-b)/2\}$ divide the plane into four regions,

labeled 1–4 in the figure. Which wave structure results from a particular (D, h_w) pair is indicated by the region in which the pair belongs, as follows:

1. For relatively small values of h_w, corresponding to region 1, a simple compressive wave arises. This wave has a capillary ridge that diminishes as D increases.
2. Within the wedge (region 2), one obtains the compressive-undercompressive double shock structure described above.
3. For large values of h_w, one obtains double wave structures involving a rarefaction fan; these are either a rarefaction-undercompressive wave when $D < D_F$ and $h_w > h_{\rm uc}$ (region 3), or
4. a rarefaction-shock wave (with a leading generalized Lax shock), for larger D (region 4).

The sketches for regions 3 and 4 in Figure 2.1 differ in the profile behind the leading undercompressive wave. In the former, the rarefaction wave separates from the leading shock, giving rise to a convex portion behind the front, while the latter profile is concave right up to the shock. In region 3, the rarefaction wave separates from the leading shock, but not in region 4. To the right of the apex ($D > D_F$) there are no structures involving undercompressive waves: above $(1 - b)/2$ there is a rarefaction-shock wave combination, while below this line a simple compressive wave occurs. Existence of undercompressive shock solutions for D less than some finite upper bound, and nonexistence for sufficiently large D, was proved by Bertozzi and Shearer [3].

We have limited the above discussion to values of $h_w > b$. In this study, the initial film profiles used have thickness $h \geq b$ everywhere, and so the thickness at later times is never much smaller than b.

In addition, we have simplified matters by neglecting the presence of a thin region of thicknesses h_w located around the lower side of the wedge. This exists for a range of D close to zero, where multiple wave structures that connect h_w to b are possible, either one of a number of compressive waves or the double shock structure. This range ends towards the right at a value D (say D_1) below two [10]. Which wave structure is selected in a numerical simulation depends on the initial profile; for monotonic initial data connecting h_w and b, a single compressive wave with the smallest capillary ridge typically arises [1, 2]. Hence for such initial data and $D < D_1$, the range of h_w for which we get a single compressive front is slightly increased above the lower edge of the wedge.

2.3. Meniscus structures. At the meniscus, the profile should become stationary after the contact line has moved away, up the inclined substrate. Hence, of primary interest here are the stationary solutions of (2.2) with far-field condition (2.3) as $x \to -\infty$ and a flat right state $h \to h_m$ for $x \to \infty$. Letting $h_t = 0$ and integrating once yields the ODE

$$h_{xxx} = Dh_x - (f(h) - f(h_m))/h^3. \tag{2.14}$$

Note that the constant of integration $Q = f(h_m)$ represents the total flux through the flat film. In earlier work [13] we investigated this boundary value problem by numerically exploring the relevant invariant manifolds in the three-dimensional phase space associated with (2.14). Solutions satisfying the far-field conditions as $x \to -\infty$ form a two-dimensional invariant manifold, while those that tend to a constant film thickness h_m as $x \to \infty$ form either a one- or a two-dimensional (stable) invariant manifold

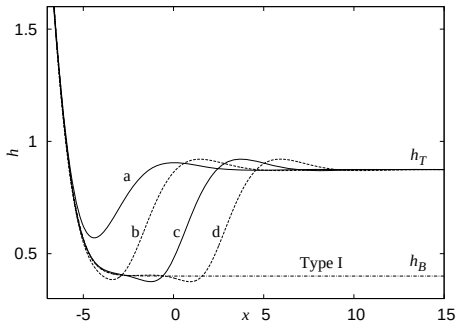

FIG. 2.2. *The first two stable and first two unstable Type* II *steady meniscus profiles, for* $D = 0.322$. *The profiles labeled a and c are stable, while b and d are unstable. Here* $h_m = h_T(0.322) = 0.8744$, *so there are an infinite number of these profiles. Also shown is the Type* I *meniscus profile for this value of D; it has* $h_m = h_B(0.322) = 0.4002$.

when either $h_m < 2/3$ or $h_m > 2/3$, respectively. Hence the stationary meniscus profiles correspond to either codimension one or codimension zero intersections of the invariant manifolds, respectively, and we call these Type I meniscus solutions in the former, and Type II meniscus solutions in the latter, case. While Type I solutions monotonically decrease in thickness as they approach h_B, Type II solutions typically have a characteristic depression or dimple in the meniscus region, particularly for sufficiently small values of D, followed by damped oscillations as $x \to \infty$ (Figure 2.2). The dimple and the oscillations can be suppressed by the normal component of gravity, i.e., for larger values of D.

The Type I solutions are structurally unstable and, for given D, exist only for discrete values of h_m. In fact, for a range of values $D < D_M = 0.8008$, numerical exploration of the phase space [13] shows that a unique Type I solution exists for a single thickness $h_m = h_B(D)$, while there are none at all for $D > D_M$. In the range $D > D_M$, Type II meniscus profiles exist for all $h_m > 2/3$, while for $D < D_M$, the situation is more complicated. We define $h_T(D)$ to be the larger positive root h of the cubic equation $f(h) = f(h_B)$, so that $h_T > 2/3$. Then Type II solutions can always be found for $h_m \geq h_T(D)$. In addition, for $D < D_B = 0.7142$, Type II solutions exist for a range of thicknesses h_m slightly below $h_T(D)$, down to a value $h_*(D)$. Moreover, when h_m is near $h_T(D)$, in the range $h_*(D) < h_m < h_{**}(D)$, with a D-dependent value $h_{**}(D) > h_T(D)$, multiple Type II solutions appear with the same thickness h_m; their profiles differ by the depth and width of the dimple, as shown in Figure 2.2. The profiles of four of the multiple Type II menisci are shown in Figure 2.2 for $D = 0.322$ and $h_m = h_T(0.322) \approx 0.8744$. (The corresponding Type I profile for this value of D is also shown.) The question of which, if any, of the Type II menisci are stable to in-plane disturbances then arises. Numerical simulations of the time-dependent PDE (2.2) revealed that these meniscus solutions are alternately stable and unstable. These simulations were initialized using the Type II profiles computed by a shooting method [13]. The unstable solutions to the ODE do not occur as solutions of the PDE at long times; instead, initial conditions which are close to these evolve toward the stable solutions. In Figure 2.2 the stable and unstable solutions are shown as solid and dashed lines, respectively.

Figure 2.3 summarizes the solution structure, showing the thicknesses $h_B(D)$ and $h_T(D)$ controlling Type I and Type II solutions in the (D, h) plane. These values

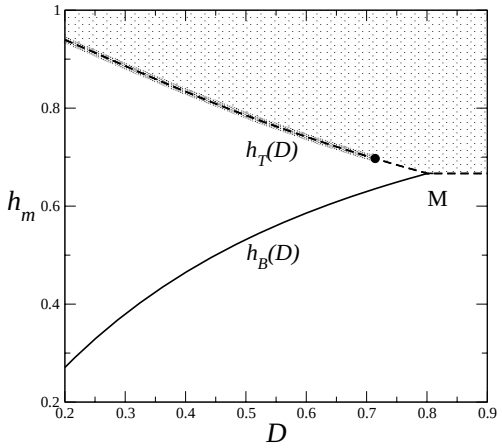

FIG. 2.3. *The meniscus wedge diagram. Lines show the allowable values for the right state of the meniscus, h_m. For $D < D_M$, the meniscus may approach a thickness h_m, where either $h_m = h_B(D)$ is given by the lower branch (a Type* I *solution) or h_m lies above the upper branch, i.e., $h_m > h_T(D)$ (a Type* II *solution). The dark shaded line indicates where multiple Type* II *menisci are possible for a range of values h_m above and below $h_T(D)$. For $D > D_M$, Type* I *solutions are not possible, but Type* II *solutions exist for all h_m above* 2/3. *The light shaded region shows where one or more Type* II *menisci are available.*

merge with $h = h_T = h_B = 2/3$ when D approaches D_M, at the point labeled M in the figure. We call the structure formed by the graphs of $h_T(D)$ and $h_B(D)$ the "meniscus wedge." Note that it does not depend on b. One or more Type II solutions exist at points in the light shaded region. The range of thicknesses with multiple Type II solutions is not precisely shown in Figure 2.3, but is indicated there by the dark shaded line along $h_T(D)$, ending in a solid dot in the figure at $D = D_B$.

3. Interaction of meniscus and front dynamics. The information summarized in section 2.2 and encapsulated in the front wedge diagram gives a fairly complete picture of which wave, or combination of waves, arises near the contact line if, for given b and D, the leftmost value of the film thickness is set at some specific value, h_w. The question of how this value is selected then arises; it is evident that the meniscus plays an important role here. If at long times, when the contact line has traveled far from the reservoir, the meniscus profile approaches a steady state, then the value of h_w must be equal to an h_m for which either a Type I or Type II solution exists. This information is found in the "meniscus wedge" diagram in section 2.3. An overview of the possible combinations of the different types of meniscus and wave structures can be obtained by superimposing the two wedge diagrams. In many cases, this suggests more than one possible outcome for a given D and b. For example, if $D < D_M$, wave structures can be found to connect either to a Type I meniscus or to a whole range of Type II menisci. However, the only situations which can arise dynamically are those for which the wave part next to the meniscus has a nonnegative speed. (If its speed were negative, such a wave part could never emerge from the meniscus.) Rarefaction waves, or parts of rarefaction waves, move with a wave speed given by characteristics, namely $f'(h)$, where the film thickness is h. For shock profiles, with left and right states h_- and h_+ the wave speed s is given by the Rankine–Hugoniot condition, $s = (f(h_+) - f(h_-))/(h_+ - h_-)$.

In this section we use such considerations to determine which meniscus and film

profile eventually evolves from monotonic initial data representing a thin precursor layer on a substrate which is partially immersed into the reservoir. The approach outlined above nearly always allows us to single out one possible scenario. The exceptions will be pointed out further below. We then verify our predictions using time-dependent simulations of (2.2). To obtain numerical solutions we use finite difference schemes on a finite spatial domain, $[0, L]$. At the left-hand boundary, we specify $h = H_0$ to be a large constant (typically 20–50) and impose $h_{xxx} = 0$. At the right-hand boundary, $h_x = h_{xxx} = 0$. Solutions are advanced in time using an implicit Euler scheme. The time step is controlled using a step-doubling approach.

Simulations began from an initial profile $h(x, 0) = h_0(x)$. The form used for h_0 was generally

$$h_0(x) = \begin{cases} D^{-3/2}\left(\exp(D^{1/2}x) - D^{1/2}x - 1\right) + b & \text{for } x \le 0, \\ b & \text{for } x > 0. \end{cases} \tag{3.1}$$

This represents the static meniscus which arises through the balance of mean surface tension and gravity for $x < 0$, and joins smoothly to the precursor layer at $x = 0$. Other initial profiles, including the function

$$h_0(x) = \frac{\log(2\cosh(ay)) - ay}{2a} + b, \tag{3.2}$$

where $y = x/D - 20$ and $a = 0.4$, were also used. This has slope -1 for $x \to -\infty$, and has $h_0 \to b$ as $x \to \infty$. We also used

$$h_0(x) = \max\left(-x/D, b\right).$$

The particular choice did not alter the qualitative behavior of the film.

As explained in section 2.2, the apex of the front wedge at $D = D_F$ moves towards smaller values of D as b is increased. Following Bertozzi, Münch, and Shearer [2], b is restricted to be less than $1/3$. Depending on b, the front wedge and meniscus wedge can therefore overlap in four characteristic arrangements, leading to four different cases. In increasing order of b, these are as follows:

A. The most important case is for small b, i.e., a very thin precursor layer. In this case D_F is large, and $h = (1-b)/2$ is close to its maximum value of $1/2$. The upper part of the front wedge $h_{\rm uc}(D)$ makes intersections with both $h_T(D)$ and $h = 2/3$. This is the arrangement which results when $b = 0.005$; it is shown in Figure 3.1(a). Here a line marked with circles indicates the left state of the advancing front h_f, while the right state of the meniscus $h_m = h_w$ is shown by crosses, for each value of D. It continues until $h_{\rm uc}(D_M, b) = 2/3$; this happens for $b = 0.0202$ (to four decimal places).

B. For larger b, the line $h_{\rm uc}(D)$ makes only one intersection with the meniscus wedge, and this is now along the lower branch $h_B(D)$. Figure 3.1(b) shows the situation for $b = 0.05$. At $b = 0.1484$, the apex of the meniscus wedge and that of the front wedge are at the same value of D, i.e., $D_F = D_M$.

C. In the third case (for $0.1484 < b < 0.2338$ to four decimal places), $D_F < D_M$, but $h_B(D_F) > (1-b)/2$, so the graph of $h_{\rm uc}(D)$ still intersects $h_B(D)$. The significance of this is explained below. Figure 3.1(c) shows this case when $b = 0.16$.

D. For the largest b ($b > 0.2338$ to four decimal places) D_F is small enough that the merger at $D = D_F$ happens with $h = (1-b)/2 > h_B(D)$, i.e., above and to the left of the line $h_B(D)$ (see Figure 3.1(d) for $b = 0.25$).

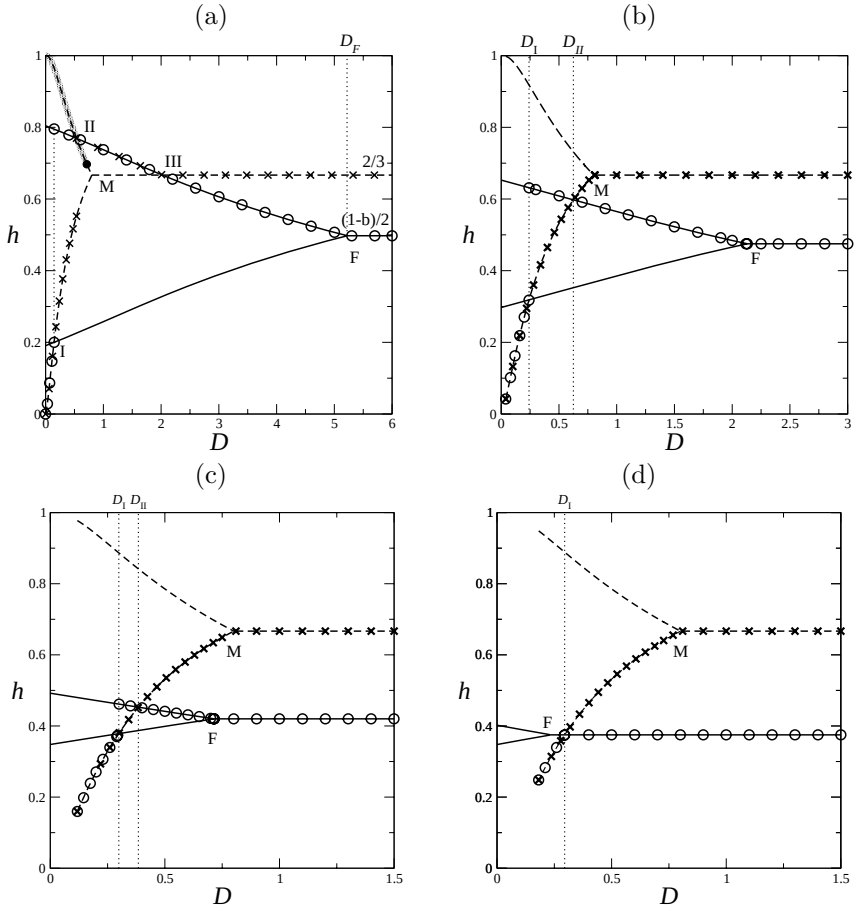

FIG. 3.1. *The (D, h) diagrams, showing the front wedge (solid lines) and meniscus wedge (dashed lines). A line marked with circles indicates the left state, h_f, of the advancing front. A line with crosses indicates the right state of the meniscus, h_m. When these lines coincide, there is a flat film region directly connecting the meniscus to the advancing front.* (a) *Case A, when $b = 0.005$;* (b) *Case B for $b = 0.05$. In* (b)*, a new profile featuring a Type* I *meniscus connected to a rarefaction fan becomes possible for D between $D_{\rm II}$ and D_M.* (c) *Case C, $b = 0.16$;* (d) *Case D, $b = 0.25$. In Case C, $D_F < D_M$, requiring a connection between h_B and $(1 - b)/2$ for $D_F < D < D_M$. In Case D, D_F is so small that the front wedge does not intersect h_B at all.*

3.1. Case A: Thin precursor layer. We first define $D_{\rm I}(b)$ to be the solutions of

$$h_B(D) = h_1(D, b) = 1 - b - h_{\rm uc}(D,\, b);$$

thus, for a given value of b, $(D_{\rm I}, h_B(D_{\rm I}))$ is the point in the (D, h) diagram where the lower sides of the two wedges intersect. We also define $D_{\rm II}(b)$ and $D_{\rm III}(b)$, denoting the solutions of

$$h_T(D) = h_{\rm uc}(D,\, b) \quad \text{and} \quad h_{\rm uc}(D, b) = \frac{2}{3},$$

respectively. These define the intersection of the upper side of the front wedge with the upper side of the meniscus wedge or the line $h = 2/3$, respectively, and are

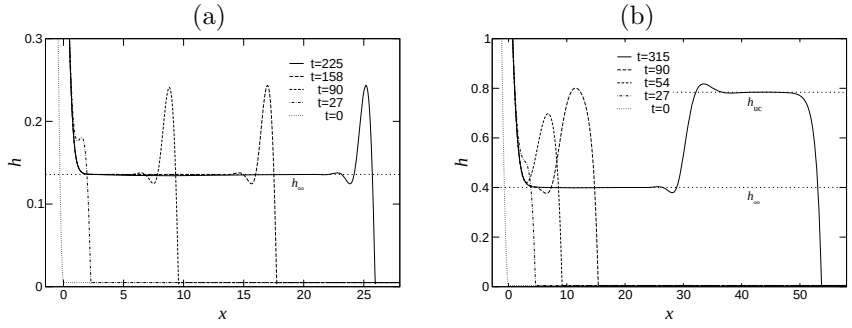

FIG. 3.2. *Numerical solutions of* (2.2) *when* (a) $D = 0.1021$ *and* (b) $D = 0.322$. *Film profiles are shown at dimensionless times given in the legends. In* (a) *there is a single compressive wave, while in* (b) *an undercompressive-Lax double shock develops and travels up the substrate. There is a thin precursor film of thickness* $b = 0.005$ *in both cases.*

shown as points II and III on Figure 3.1(a). When $b = 0.005$, the numerical value for $D_{\rm I} = 0.1461$. The other special values of D given in this section are also for $b = 0.005$.

We begin with the smallest D (but sufficiently large that $h_B > b$) and argue that the meniscus must be of Type I there. First, consider values of $D < D_{\rm I}$. Suppose that the meniscus is of Type II, with a right state thickness $h_m \geq h_T$. In this range of D, h_T in turn is larger than $h_{\rm uc}$. A connection from h_m to the precursor would involve a rarefaction fan followed by an undercompressive wave joining to b. However, the left part of the rarefaction fan would have negative speed, and therefore would fall back into the meniscus. Hence such a solution cannot persist.

On the other hand, if the meniscus is of Type I, then $h_m = h_B < h_1$, and a simple compressive connection to the precursor is possible. This is connected by a flat film to a steadily advancing front. The left state of the advancing front and the right state of the meniscus are identical in this case, since the two are directly connected. Our dynamical simulations for $D = 0.1021 < D_{\rm I}$ and $b = 0.005$ (Example 1 in [13], also shown in Figure 3.2(a)) confirm that this combination of Type I meniscus and a simple compressive wave occurs. The flat region thickness in this case is controlled by the meniscus.

When D is increased above $D_{\rm I}$, the graph of $h_B(D)$ enters the undercompressive region of the front wedge. In place of a simple compressive connection, a Type I meniscus must now connect to a double shock structure. A Type II meniscus is still not possible, for the same reason as in the previous case, namely that $h_T > h_{\rm uc}$ while $D < D_{\rm II}$. Now the left state of the advancing front is the undercompressive wave height $h_{\rm uc}$. The flat region ahead of the meniscus, with thickness h_B, is connected to $h_{\rm uc}$ by the trailing compressive part of the double wave structure. This trailing shock moves upwards, but somewhat slower than the advancing front. In the (D, h) diagram, Figure 3.1(a), the line marked by circles jumps to $h_{\rm uc}$ at $D = D_{\rm I}$, separating from the line portion emphasized by crosses.

In section 2.2 it was noted that when D is small, compressive waves exist for $h_w < h_{ii}$, where h_{ii} is slightly larger than h_1. For $h_1 < h_w < h_{ii}$, the meniscus can be connected to either a double shock structure or to one of several compressive waves. These all have positive wave speeds, and which one is selected depends on the initial data. Due to the experience with monotonic (jump) initial data, we expect that the simplest compressive wave is selected if $h_B < h_{ii}$. The net effect of this is that, for the initial profiles considered in this paper, the transition from a compressive front to

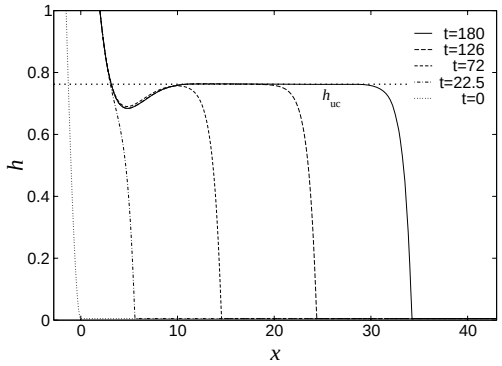

FIG. 3.3. *Evolution of* (2.2) *for* $D = 0.6424$ *at dimensionless times given in the legends. Only the undercompressive shock propagates away from the meniscus, which evolves into a Type* II *meniscus. Again the precursor layer thickness is* $b = 0.005$.

a double shock is delayed and occurs for a value D_I' slightly larger than D_I. Indeed, for $b = 0.005$ we find that this transition occurs for D between 0.16 and 0.18, instead of precisely at $D_{\mathrm{I}} = 0.1461$.

This behavior continues until $D = D_{\mathrm{II}}$, the value of D at which $h_{\mathrm{uc}} = h_T$ and the upper sides of the two wedges cross. For $b = 0.005$, D_{II} equals 0.535. A double shock structure moving up the substrate is shown for $D = 0.322$ in Example 2 of [13], and also in Figure 3.2(b) just as we described it here.

For $D_{\mathrm{II}} < D < D_{\mathrm{III}}$, h_{uc} is larger than h_T, and so it is in the region where Type II meniscus solutions are possible. Hence a direct undercompressive shock connection from a Type II meniscus to the precursor is possible. (The existence of multiple Type II solutions for h near h_T means that a Type II solution is available for matching to h_{uc} via a direct connection at values of D slightly below D_{II}.) These continue until $D = D_{\mathrm{III}}$; for $b = 0.005$, $D_{\mathrm{III}} = 2.025$. For $D < D_{\mathrm{III}}$, h_{uc} is larger than 2/3. Thus we can rule out connections involving intermediate waves as follows. Only shocks can connect to h_{uc} from below (since characteristics for the left and right state would cross, ruling out a rarefaction fan), and these would have a negative speed. Similarly, any wave connection from above must be a rarefaction fan, all parts of which would also have a negative speed.

As a result, the only structure possible is a Type II meniscus connecting directly to a flat state with thickness h_{uc}. This flat state is the left state of an undercompressive shock connection to the precursor. The right state of the meniscus and the left state of the advancing front are again identical, and in Figure 3.1(a) the lines marked by crosses and circles coincide. It is notable that in this range of D the thickness of the flat region, h_{uc}, is determined by the precursor thickness, not by the meniscus. We therefore refer to these structures as "front controlled." This situation in this range is exactly what is observed for Example 3 from [13] and in Figure 3.3, where $D = 0.6424$.

Once again, this description has to be slightly amended. The reason is that, for $D < D_B = 0.7142$, Type II menisci exist even for h_m below h_T (down to the value h_* introduced in section 2.3). Hence, in principle, they can arise and connect directly to an advancing front for values slightly smaller than D_{II}, as an alternative to a double shock structure rising from a Type I meniscus. Furthermore, in the range from h_* to $h_{**} > h_T$, mentioned in section 2.3, different Type II meniscus solutions sharing the

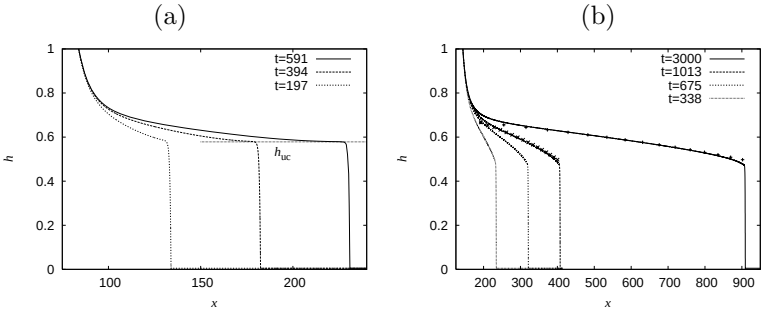

FIG. 3.4. (a) *Evolution of* (2.2) *when* $D = 3.5$ *and* $b = 0.005$*, so* $D < D_F$*. The front is undercompressive. A small flat region of thickness* $h_{\rm uc}$ *(indicated by a dotted line) gradually develops behind the front.* (b) *With* D *increased to* 6*, larger than* D_F*, the front is a generalized Lax shock. The rarefaction fan is also shown at* $t = 3000$ (+ *symbols*) *and* $t = 1013$ (×)*; it was obtained by solving the scalar hyperbolic conservation law as described in detail in section* 4.

same value for h_m exist. Hence, in the thin range of values of D for which $h_{\rm uc}(D, b)$ lies between the graphs of $h_*(D)$ and $h_{**}(D)$, the combination of the wedge diagrams and the criterion for the wave speeds is not sufficient to predict the film behavior. Instead behavior can be determined by, e.g., numerical simulations. We will not elaborate further on this subtlety.

For the small values of D considered so far, there is in fact a distinct flat region between the meniscus and the wave structure. For larger D, this is not so. As D increases beyond $D_{\rm III}$, the height of the left state for an undercompressive front $h_{\rm uc}$ drops below $h = 2/3$. Now there can be no direct connection between meniscus and front. All available meniscus profiles have h_m larger than $h_{\rm uc}$, so an intermediate wave is needed to span the gap of thicknesses. From the front wedge part in Figure 2.1, we see that the resulting wave structure must be a rarefaction-undercompressive wave combination.

No flat film can emerge between the meniscus and the rarefaction wave of thickness $h_m = h_w$ strictly larger than $2/3$, since the portions of the rarefaction wave larger than $2/3$ would have a negative characteristic speed. Instead, the meniscus evolves into a shape that is the limiting profile of all the Type II menisci, while the portions of the film between $2/3$ and $h_{\rm uc}$ tend to the profile of a rarefaction wave with left state $2/3$. Since the characteristic speed at $h = 2/3$ is exactly zero, the rarefaction wave never completely separates from the meniscus, but as it gets increasingly stretched, the film thickness at any fixed position x in front of the meniscus eventually tends to $2/3$. We call the emerging limiting meniscus profile with thickness $h_m = 2/3$ a *generalized Type II meniscus*, in analogy to the terminology for Lax shocks, to reflect the fact that $f'(2/3) = 0$.

This situation is indicated in Figure 3.1(a), where for $D > D_{\rm III}$ the crossed and circled lines part again. The former lies at the boundary of the Type II regime, while the latter follows the upper edge of the front wedge. Dynamical simulations with $D = 3.5$ confirm our picture. In Figure 3.4(a) we show the evolution of the film from the initial condition (3.2), for $D = 3.5$. At long times, the film left of the advancing front forms a flat plateau with thickness equal to $h_{\rm uc} = 0.5783$ (the value was obtained by solving the traveling wave ODE as in [2, 10]). At an increasing distance from the advancing front, the film profile slightly steepens to a rarefaction wave, which blends over into the meniscus.

When D increases further, $h_{\rm uc}$ decreases, and the difference between the speed of the undercompressive wave and the left characteristic speed of this wave also decreases. They become equal when $D = D_F$ and $h_{\rm uc} = (1-b)/2$ at the apex of the front wedge. For $b = 0.005$, D_F is 5.227. For the largest D, in excess of D_F, the possible wave structures are those that are permitted according to classical shock theory.

Again, the meniscus profile tends to a generalized Type II meniscus, and it must connect to a rarefaction fan with left state 2/3. The rarefaction wave now connects directly to the advancing front, which connects in turn to b. The characteristic speed of the thickness $(1-b)/2$ where the two structures connect is identical to the shock speed. The leading shock is therefore a generalized Lax shock, which is not undercompressive, and there is neither the flat region of thickness $h_{\rm uc}$ nor the steep shock front which were visible when $D = 3.5$. This is seen in a dynamical simulation for $D = 6$ in Figure 3.4(b). Instead, the rarefaction fan expands over time, always stretching from the meniscus to the advancing front. The front is a generalized Lax shock and connects to the rarefaction fan via a rounded corner at thickness $h = (1-b)/2 = 0.4975$.

3.2. Case B: Thicker precursor layer, $0.0202 < b < 0.1484$. For larger precursor thicknesses, the expected film configuration is generally similar to the small b case described above. However, some new configurations do appear for a range of D values, while the front controlled profiles with a Type II meniscus and flat region thicker than 2/3 no longer occur.

The intersections occurring at $D = D_{\rm II}$ and $D = D_{\rm III}$ both happen at $D = D_M$ when $b = 0.0202$. For larger b, the upper branch $h_{\rm uc}$ of the front wedge intersects only the lower branch of the meniscus wedge. We call the value of D for the remaining intersection $D_{\rm II}$, and so

$$h_B(D_{\rm II}) = h_{\rm uc}(D_{\rm II}, b)$$

for this range of b. The two wedges are shown for $b = 0.05$ in Figure 3.1(b). We describe below the profiles which result as D is increased.

For $D < D_{\rm II}$, the film behaves as for the first two cases in Case A (section 3.1). For the smallest D, profiles continue to be controlled by the meniscus, with a Type I meniscus, a flat region of thickness h_B, and simple compressive front, with a capillary ridge connecting the flat region to the precursor layer. When $D_{\rm I} < D < D_{\rm II}$, there are again a Type I meniscus and flat region with thickness h_B, but at the advancing front there is a double shock structure. Both these behaviors have been seen in our dynamic simulations with $b = 0.05$.

Because $h_{\rm uc}(D)$ is smaller than in Case A for the larger values of b considered here, it never exceeds h_T, the threshold for a Type II meniscus. (See Figure 3.1(b).) Thus for this range of b there are no front controlled profiles. Instead, for $D_{\rm II} < D < D_M$, a new configuration is possible. Now both h_B and h_T are greater than $h_{\rm uc}$, so any connection from the meniscus must be via a rarefaction fan. This cannot connect to a Type II meniscus, since $h_T > 2/3$, and so the left part of the rarefaction would have negative speed. Thus here there is a Type I meniscus, connected via a rarefaction fan to a flat region of height $h_{\rm uc}$ where the film is thinner. This in turn is connected via an undercompressive shock to b. All parts of the rarefaction wave have positive speed, so it must gradually move away from the meniscus, leaving a flat region of thickness h_B behind it. Furthermore, the leading edge of the rarefaction fan is slower than the undercompressive wave, so the length of the flat region between the rarefaction fan leading edge and the advancing front, with thickness $h_{\rm uc}$, will increase with time. Dynamical simulations with $D = 0.7$ and $b = 0.05$, shown in Figure 3.5(a), confirm

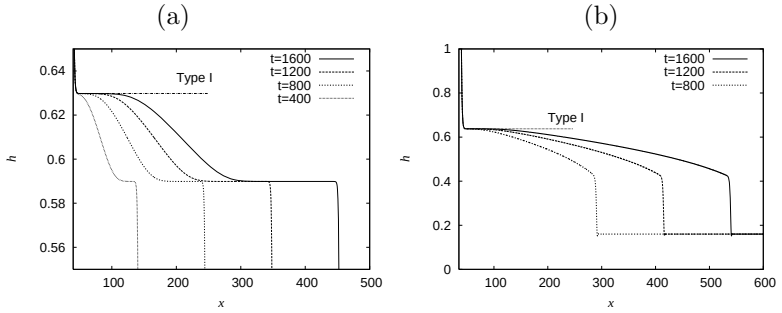

FIG. 3.5. (a) *Evolution of the film when* $D = 0.7$ *and* $b = 0.05$ *(so* $D_{\rm II} < D < D_M$*). A Type* I *meniscus, which tends towards* $h_B = 0.6298$*, is connected via a rarefaction fan to a flat region of height* $h_{\rm uc}$*, which connects to the precursor thickness* b *via an undercompressive shock. This configuration is possible only when* $b > 0.0202$*.* (b) *Evolution of the film when* $D = 0.72$*. Here* $b = 0.16$*. The front is now a generalized Lax shock, unlike that seen in the left figure. The meniscus is still Type* I*, approaching a value* $h_B = 0.6376 < 2/3$*. A knee develops close to* $h = (1-b)/2 = 0.42$*.*

that two flat regions develop. The first has thickness close to $h_B = 0.6298$, as expected for a Type I meniscus solution for this value of D, and extends up to the rarefaction fan. A second develops between the rarefaction fan and the advancing front, with a thickness close to the expected undercompressive region height $h_{\rm uc} = 0.5907$.

For $D > D_M$, the behavior is similar to that for $D > D_{\rm III}$ for small b (section 3.1). There is a rarefaction fan extending from a generalized Type II meniscus at $h = 2/3$ to $h_{\rm uc}$. Provided that $D < D_F$, a flat region of thickness $h_{\rm uc}$ exists before an undercompressive shock, while for $D > D_F$ there is no flat region, and the connection to the precursor is a generalized Lax shock.

3.3. Case C: Even thicker precursor layer, $0.1484 < b < 0.2338$. As b is further increased, D_F reduces, so that when it reaches the critical value $b = 0.1484$, D_F and D_M are equal. For somewhat larger b (so that $D_F < D_M$, but is not too small) the apex of the front wedge still lies outside the meniscus wedge. This arrangement of the wedges is shown in Figure 3.1(c) when $b = 0.16$.

With this arrangement, the film behaves as for Cases A and B while $D < D_{\rm II}$, forming a Type I meniscus with a compressive shock for $D < D_{\rm I}$, and then a double shock for $D_{\rm I} < D < D_{\rm II}$. For $D > D_{\rm II}$ but less than D_F, the Type I meniscus still exists and connects to the precursor via a flat region of thickness h_B, then a rarefaction fan and undercompressive shock, as in Case B. In dynamic simulations the flat $h_{\rm uc}$ region takes a long time to develop.

For $D_F < D < D_M$ another new behavior occurs. Type I menisci are still possible, but they must connect to the precursor by a rarefaction fan with right state $(1-b)/2$, followed by a classical generalized Lax shock, since undercompressive connections do not exist for $D > D_F$. Such behavior is seen in Figure 3.5(b), for $D = 0.72$ and $b = 0.16$. (Note that $D_F = 0.7153$ for $b = 0.16$.) Here $h_B = 0.6376$, and it is apparent that in the meniscus region the film approaches this thickness before entering the rarefaction fan region and dropping to $(1-b)/2 = 0.42$. Since h_B is quite close to $2/3$ here, characteristics have a slow speed, and the left edge of the rarefaction fan takes a long time to move away from the meniscus. Finally, for $D > D_M$, behavior is again as for the largest D values in Cases A and B: a generalized Type II meniscus connects to a rarefaction fan and from there to a generalized Lax shock, as in Figure 3.4(b).

3.4. Case D: Thickest precursor layers: $b > 0.2338$. With this arrangement of the wedges, $D_F < D_{\mathrm{I}}$, and the front wedge lies entirely within the meniscus wedge. Figure 3.1(d) shows the case $b = 0.25$. Three types of behavior are possible; these are similar to those of Case C.

For small $D < D_{\mathrm{I}}$ (but sufficiently large that $h_B > b$), the film continues to display meniscus-controlled behavior. There is a Type I meniscus, followed by a flat region with thickness $h_B(D)$, which is connected to the precursor layer by a compressive advancing front. This is the case, regardless of whether D is larger or smaller than D_F.

When $D > D_{\mathrm{I}}$, the connection to the precursor must be via a classical structure (since $D_{\mathrm{I}} > D_F$). Since the preferred right state of the meniscus exceeds $(1 - b)/2$, there is a rarefaction fan, connecting to a classical generalized Lax shock. The two behaviors possible for $D > D_{\mathrm{I}}$ differ near the meniscus: for $D_{\mathrm{I}} < D < D_M$, it is a Type I meniscus, which connects to the rarefaction fan as in section 3.3. Once D exceeds D_M, there is a generalized Type II meniscus that joins to the rarefaction fan, as for the largest D values in the previous cases.

4. Nearly horizontal substrate: Large D. For a substrate which is nearly horizontal, the leveling effects of the normal component of gravity become important. Here we consider steady state profiles in the limit $D \to \infty$. For studying this regime, we adopt a scaling in which surface tension is neglected but both components of gravity are retained. Smoothing of discontinuities in the film is now provided by the normal component of gravity instead of predominantly by surface tension. Rescaling by defining $\tilde{x}$ and $\tilde{t}$ by

$$D\tilde{x} = x, \qquad D\tilde{t} = t, \tag{4.1}$$

and letting $D \to \infty$ causes the governing PDE (2.2) to reduce from fourth to second order:

$$h_{\tilde{t}} + \left(h^2 - h^3\right)_{\tilde{x}} = \left(h^3 h_{\tilde{x}}\right)_{\tilde{x}}. \tag{4.2}$$

Steady state solutions of (4.2), which represent feasible meniscus profiles, must satisfy boundary conditions far upstream and downstream. The film must match onto the reservoir, so

$$\frac{\mathrm{d}h}{\mathrm{d}\tilde{x}} \to -1 \qquad \text{as } \tilde{x} \to -\infty$$

(which is simply the rescaled form of (2.3)), and its thickness must approach a constant value h_m far downstream:

$$h \to h_m \qquad \text{as } \tilde{x} \to \infty.$$

Setting $h_{\tilde{t}}$ to zero, (4.2) can be integrated with respect to $\tilde{x}$ to yield a first-order (nonlinear) ODE:

$$h_{\tilde{x}} = \frac{h^2 - h^3 - c}{h^3}. \tag{4.3}$$

For large h, equation (4.3) has $h_{\tilde{x}} \to -1$, and by setting the constant of integration $c = (h_m^2 - h_m^3)$, both boundary conditions are satisfied. Note that c is the total flux of liquid flowing through the flat film in front of the meniscus; physically meaningful

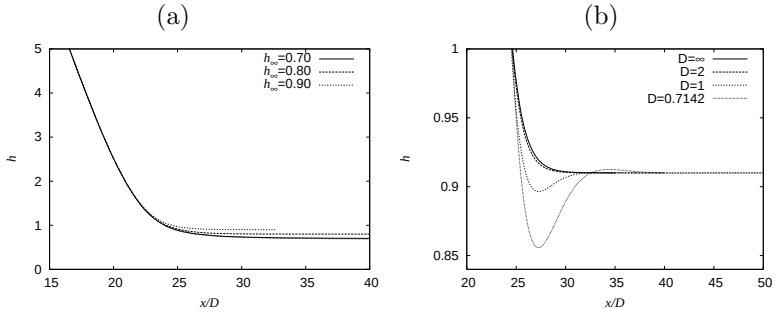

FIG. 4.1. (a) *Solutions of* (4.3) *in a parameter regime where surface tension is unimportant. Shown are* $h_m = 0.7, 0.8, 0.9$. *On this scale, the solution with* $h_m = 0.7$ *is barely distinguishable from the solution of* (4.5) *with* $h_m = 2/3$, *shown as a dotted line.* (b) *Steady solutions of* (2.2), *which have* $h_m = 0.91$, *rescaled according to* (4.1). *As* D *is increased, these approach the large* D *limit, shown as a solid line. The dip which is a feature of Type* II *solutions for small* D *is gone for* $D = 2$.

values for climbing films are $0 < c \leq 4/27$. A one-parameter family of solutions is generated by varying h_m, or alternatively, c. For $c < 4/27$, the positive-valued fixed points of (4.3) are $h = h_B < 2/3$ and $h = h_T > 2/3$, the same as those of the steady form of (2.2).

When h_B and h_T are distinct, (4.3) shows that $h_{\tilde{x}}$ is negative for $h > h_T$ and $h < h_B$, and positive for $h_B < h < h_T$; h_T is therefore a stable fixed point, while h_B is unstable. Any solution which becomes infinite as $\tilde{x} \to -\infty$ must be monotonic, decreasing, and have $h > h_T > 2/3$ everywhere, with $h \to h_T$ as $\tilde{x} \to \infty$. In other words, the meniscus profiles for $c < 4/27$ connect to a thickness $h_m > 2/3$, and so are Type II profiles. The exact solution to (4.3), up to translation in $\tilde{x}$, is given implicitly by

$$\tilde{x} = -h + \sum_{i=1}^{3} \frac{h_i^3}{(h_i - h_j)(h_k - h_i)} \log|h - h_i|, \qquad j \neq i,\ k \neq i, j, \tag{4.4}$$

where the summation is over the three distinct roots h_B, h_T, and $(1 - h_B - h_T)$ of the cubic equation $h^2 - h^3 - c = 0$. Solutions of the form of (4.4) are shown in Figure 4.1(a) for three values of $h_m > 2/3$. The solution with $h_m = 0.91$ is compared to meniscus profiles with finite D in Figure 4.1(b). As the influence of surface tension diminishes, the dip disappears, and the meniscus profiles become monotonic, even though they are of Type II.

As h_m approaches $2/3$, the fixed points h_B and h_T also approach $2/3$. When $h_m = 2/3$, $c = 4/27$, and there is a repeated root of $h^2 - h^3 - c = 0$. The solution to (4.3) is then given by

$$\tilde{x} = -h + \frac{8}{27}\frac{1}{h - 2/3} - \frac{28}{27}\log\left|h - \frac{2}{3}\right| + \frac{1}{27}\log\left|h + \frac{1}{3}\right|. \tag{4.5}$$

The $(h - 2/3)^{-1}$ term rapidly blows up, indicating that the film requires a very long distance to reach its limiting value h_m. The solution for $h_m = 2/3$ is shown in Figure 4.1(a) as a dotted line.

At this point, we have established essentially the same picture for the possible meniscus structure as for the large (but finite) D case discussed in section 3. On

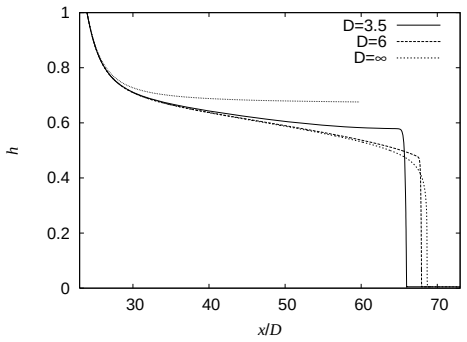

FIG. 4.2. *Advancing fronts with $b = 0.005$ and different D, shown at the same scaled time $\tilde{t} = 169$. Also shown is the long-time solution for $h_m = 2/3$ and $D = \infty$ (dotted line), which is approached by the solutions for large D, and when the front has moved far from the meniscus.*

the other hand, since (4.2) is a second-order equation, the classical theory of shocks only allows a rarefaction fan and generalized Lax shock combination for connecting a thickness larger than $(1-b)/2$ with a precursor of thickness b. Therefore in numerical simulations of (4.2) a generalized Type II meniscus profile should emerge connected to such a combination, and indeed, this is seen in the results of the previous section for sufficiently large D.

We compared the profiles obtained from our dynamic model including the surface tension terms (2.2) for two moderately large values of D with those of the time-dependent model (4.2) valid when $D \to \infty$. Simulations were performed with $b = 0.005$, for which $D_F \approx 5.227$. The same initial condition (3.2) was used for each case.

As described in section 2.2, when D is larger than D_F, the presence of the surface tension terms is expected to give rise to a classical front, with a rarefaction fan connected to a compressive shock. Numerical simulations with $D = 6$ confirm this. This is shown in Figure 3.4(b), where the front advances with a rounded corner, typical of a generalized Lax shock. In contrast, when $D = 3.5 < D_F$ the advancing front is undercompressive (Figure 3.4(a)). It separates from the rarefaction wave and has a markedly higher left state. At the same rescaled time $\tilde{t} = 169$, the rescaled profiles for the meniscus region and much of the film are very similar to the large D result, i.e., using (4.2), for both finite D values. This is shown in Figure 4.2. However, at the advancing front, the difference between the undercompressive and generalized Lax fronts is evident, while the transition from generalized Lax shock to the precursor is slightly more rounded for $D = 6$ than for $D = \infty$.

Finally, we demonstrate that the portion behind the advancing front seen in Figure 3.4(b) (and also Figure 3.5(b)) is indeed a rarefaction fan, by comparing it directly to solutions of the first-order equation resulting from neglecting all second- and fourth-order smoothing terms in (2.2). Rarefaction wave solutions of $h_t + f(h)_x = 0$ may be found, subject to appropriate initial data, using the method of characteristics. Thus within the rarefaction fan delimited by left and right states h_- and h_+,

$$h(x,t) = h_R(\xi) = (f')^{-1}(\xi), \quad \text{where } \xi = \frac{x - x_0}{t - t_0} \tag{4.6}$$

for some x_0 and t_0. The function $h_R(\xi)$ is given implicitly by $\xi = f'(h) = 2h - 3h^2$. The unknowns x_0 and t_0 may be estimated as follows. For the situation shown in Figure 3.4(b), we take h_+ to be $(1-b)/2 = 0.4975$. At a given time, t_2 say, we observe

where $h(x, t_2) = h_+$, at $x = x_+$ say, and estimate a value for t_0. We then compute

$$x_0 = x_+ + (t_2 - t_0)\xi_+,$$

where $\xi_+ = f'(h_+)$. The shape of the rarefaction fan may be constructed at any time t using

$$x = (t - t_0)\xi(h) + x_0 \quad \text{for } h_+ < h < 2/3. \tag{4.7}$$

We vary t_0 until (4.7) provides a good fit for $h(x, t_2)$ within the rarefaction fan.

We demonstrate this by computing the rarefaction fan constants x_0 and t_0 using our result at $t = 3000$ (shown using "+" symbols in Figure 3.4(b)) and then confirming these by comparison with (4.7) at $t = 1013$ ("×" symbols in Figure 3.4(b)). The agreement is satisfactory in the interior of the rarefaction fan. At the ends, the higher-order terms in (2.2) are important and smooth the profile.

5. Summary of behavior: A catalog. The previous sections' observations can be summarized by considering regions of (D, b) parameter space in which distinct behaviors arise. These are shown in Figure 5.1. The graphs of $D_i(b)$ $(i = \mathrm{I}, \mathrm{II}, \mathrm{III})$ and $D_F(b)$ divide the parameter space into several regions. These regions are indicated by the labels in the figure. The descriptions given for Cases A to D in section 3 correspond to moving along horizontal lines (constant b) in this figure.

A number of features are apparent. For small D (though with $D \gg \epsilon$), a Type I meniscus (labeled "T1+L") results for all choices of b. At the other extreme, for the largest $D > \max(D_F, D_M)$, the advancing front is a generalized Lax shock, and the connection to the meniscus is via a rarefaction fan (labeled "2/3+rf+gL"). States in

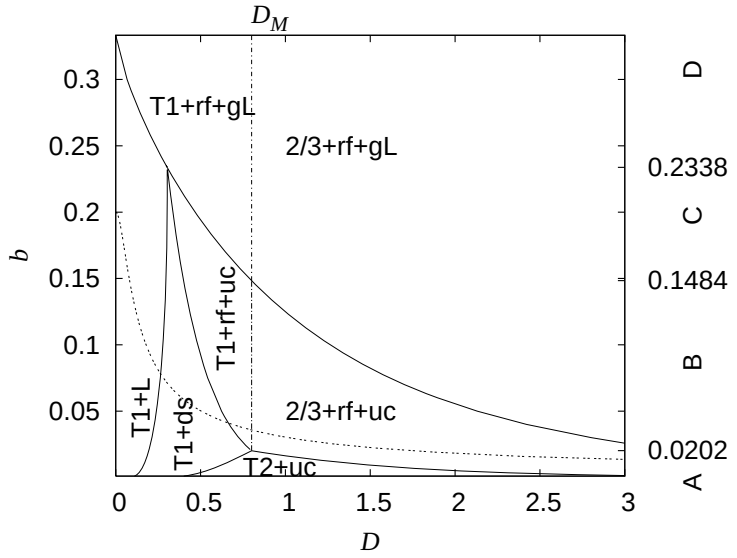

FIG. 5.1. *Behavior of a thin surface-tension-gradient-driven film emerging from a meniscus. The thickness b of a thin precursor layer and an inclination parameter D control the behavior. The following abbreviations are used, and explained in the text: T1, T2, and 2/3 denote Type* I, *Type* II, *and 2/3 (generalized Type* II*) menisci, respectively; the other labels are: L—(compressive) Lax shock, ds—double shock, gL—generalized Lax shock, rf—rarefaction fan, uc—undercompressive shock. The dotted line indicates points which differ only in tilt angle* α.

which there is only a flat region between the meniscus and front—the Type I meniscus with a Lax front or with a double shock structure, and the Type II meniscus with an undercompressive front—exist in the lower left part of the diagram, shown by labels "T1+L," "T1+ds," and "T2+uc." These are states are familiar from previous work, e.g., [13]. For a fixed value of D, one of these three configurations can arise only when a sufficiently thin precursor is present. As the precursor layer is thickened these give way to film profiles with rarefaction fans, shown by "rf" in the figure labels. These new kinds of behavior were described in section 3. In particular, the combination of a Type I meniscus and rarefaction fan seen in Figure 3.5(a) occurs only for $b > 0.0202$, while a Type II meniscus with an extended flat region and undercompressive front occurs only for b smaller than this value. In the upper right part of the diagram lie structures with rarefaction fans, for which there is no clear separation between the meniscus and the front.

It should be noted that in a set of experiments, the dimensional precursor thickness b^* (or equivalently the wetting behavior) is likely to be fixed. If the substrate angle α is varied while other parameters including b^* are fixed, then this corresponds to moving along a curved path in Figure 5.1, given parametrically by $((3\delta)^{2/3} \sin\alpha/\cos^{4/3}\alpha,\, b_0 \cos\alpha)$, where b_0 is the dimensionless precursor thickness for $\alpha = 0$. One such curve is shown in the figure for $\delta = 0.00782$, corresponding to experiments by Schneemilch and Cazabat [14], and $b_0 = 0.2$, as a dotted line. This value is likely to be larger than in their experiments, but demonstrates how the film changes from a Type I meniscus and compressive front to more complex behavior as α is increased. For this value of δ, values of $b_0 > 0.11$ result in not entering the "T2+uc" region for any α.

6. Concluding remarks. In this paper, understanding of the film on a heated tilted substrate near a meniscus and at an advancing front has been combined to generate an understanding of the possible behavior for the entire film. This is graphically summarized by Figure 5.1. This analysis is based on approximating the curvature, which is appropriate for relatively tilted substrates, for which $\tan\alpha \gg 1$. This is equivalent to requiring that $D \gg \epsilon$.

When D is of order ϵ or smaller, the curvature can no longer be approximated by h_{xx} everywhere. In this limit h_B approaches a finite nonzero value [4, 5, 11, 13]. For practical values of the shear stress, the most significant effect is to move the bottom edge of the meniscus wedge so that the graph of $1 - b - h_{\rm uc}$ no longer intersects $h_B(D)$. This situation occurs more easily for smaller values of b. In that case, instead of a Type I meniscus with a compressive front for the smallest values of D, either a double shock profile or a Type II meniscus with undercompressive front may occur. In principle, this means that undercompressive advancing fronts are possible for nearly vertical substrates, provided that the precursor layer is sufficiently thin. Retaining full curvature would modify the results shown in Figure 5.1 for D near 0.

Our results indicate that when the control parameter D is sufficiently large there is no extended flat region, but rather a rarefaction fan links the meniscus to the advancing front. An interesting observation is that when a Type II meniscus arises, its flat region thickness is not controlled by conditions at the meniscus, as for the Type I meniscus. Rather, it is the precursor thickness which determines $h_{\rm uc}$ and so the thickness of the flat region.

Similarly the interesting question of what would happen if the film were to advance over a substrate for which wetting is imperfect, i.e., for which there is a nonzero contact angle, has not been addressed. For the drag-out problem, there is a minimum

withdrawal speed required to draw out a film, if the contact angle is prescribed [7].

Despite these limitations, we expect that the guide presented here will be a useful tool for experimentalists. We look forward to experimental confirmation of these results.

REFERENCES

[1] A. L. Bertozzi, A. Münch, X. Fanton, and A. M. Cazabat, *Contact line stability and 'undercompressive shocks' in driven thin film flow*, Phys. Rev. Lett., 81 (1998), pp. 5169–5172.

[2] A. L. Bertozzi, A. Münch, and M. Shearer, *Undercompressive waves in driven thin film flow*, Phys. D, 134 (1999), pp. 431–464.

[3] A. L. Bertozzi and M. Shearer, *Existence of undercompressive traveling waves in thin film equations*, SIAM J. Math. Anal., 32 (2000), pp. 194–213.

[4] P. Carles and A.-M. Cazabat, *The thickness of surface-tension-gradient-driven spreading films*, J. Colloid Interface Sci., 157 (1993), pp. 196–201.

[5] X. Fanton, A.-M. Cazabat, and D. Quéré, *Thickness and shape of films driven by a Marangoni flow*, Langmuir, 12 (1996), pp. 5875–5880.

[6] R. P. Haskett, T. P. Witelski, and J. Sur, *Localized Marangoni forcing in driven thin films*, Phys. D, 209 (2005), pp. 117–134.

[7] L. M. Hocking, *Meniscus draw-up and draining*, European J. Appl. Math., 12 (2001), pp. 195–208.

[8] R. Levy and M. Shearer, *Kinetics and nucleation for driven thin film flow*, Phys. D, 209 (2005), pp. 145–163.

[9] O. K. Matar and R. V. Craster, *Models for Marangoni drying*, Phys. Fluids, 13 (2001), pp. 1869–1883.

[10] A. Münch, *Shock transitions in Marangoni-gravity driven thin film flow*, Nonlinearity, 13 (2000), pp. 731–746.

[11] A. Münch, *The thickness of a Marangoni-driven thin liquid film emerging from a meniscus*, SIAM J. Appl. Math., 62 (2002), pp. 2045–2063.

[12] A. Münch, *Pinch-off transition in Marangoni-driven thin films*, Phys. Rev. Lett., 91 (2003), paper 016105.

[13] A. Münch and P. L. Evans, *Marangoni-driven liquid films rising out of a meniscus onto a nearly horizontal substrate*, Phys. D, 209 (2005), pp. 164–177.

[14] M. Schneemilch and A. M. Cazabat, *Shock separation in wetting films driven by thermal gradients*, Langmuir, 16 (2000), pp. 9850–9856.

[15] M. Schneemilch and A. M. Cazabat, *Wetting films in thermal gradients*, Langmuir, 16 (2000), pp. 8796–8801.

[16] L. W. Schwartz, *On the asymptotic analysis of surface-stress-driven thin-layer flow*, J. Engrg. Math., 39 (2001), pp. 171–188.